

Green Chemistry

Accepted Manuscript



This article can be cited before page numbers have been issued, to do this please use: R. Nie, H. Yang, H. Zhang, X. Yu, X. Lu, D. Zhou and Q.-H. Xia, *Green Chem.*, 2017, DOI: 10.1039/C7GC00531H.



This is an Accepted Manuscript, which has been through the Royal Society of Chemistry peer review process and has been accepted for publication.

Accepted Manuscripts are published online shortly after acceptance, before technical editing, formatting and proof reading. Using this free service, authors can make their results available to the community, in citable form, before we publish the edited article. We will replace this Accepted Manuscript with the edited and formatted Advance Article as soon as it is available.

You can find more information about Accepted Manuscripts in the [author guidelines](#).

Please note that technical editing may introduce minor changes to the text and/or graphics, which may alter content. The journal's standard [Terms & Conditions](#) and the ethical guidelines, outlined in our [author and reviewer resource centre](#), still apply. In no event shall the Royal Society of Chemistry be held responsible for any errors or omissions in this Accepted Manuscript or any consequences arising from the use of any information it contains.



Green Chemistry

PAPER

Mild-temperature hydrodeoxygenation of vanillin over porous nitrogen-doped carbon black supported nickel nanoparticles †

Received 00th January 20xx,
Accepted 00th January 20xx

DOI: 10.1039/x0xx00000x

www.rsc.org/

Renfeng Nie, Huanhuan Yang, Haifu Zhang, Xiaolong Yu, Xinhuan Lu, Dan Zhou* and Qinghua Xia*

Porous nitrogen-doped carbon black (NCB) is synthesized by facile carbonization of carbon black (CB) coated with polypyrrole (CB@polypyrrole) and used as support for Ni nanoparticles (NPs). Microstructure, reducibility and crystallinity of as-synthesized materials are investigated by transmission electron microscope (TEM), H₂-TPR/TPD, X-ray photoelectron spectroscopy (XPS) and X-ray diffraction (XRD), respectively. It is found that surface nitrogen species on NCB significantly promote the decomposition of the nickel precursor and the reduction of nickel oxide, and improve the stability of metallic Ni in ambient atmosphere. In the selective hydrodeoxygenation (HDO) of vanillin in aqueous phase at low hydrogen pressure (0.5 MPa) and mild temperature (<150 °C), Ni/NCB shows much higher activity than those of N-free catalysts, which is ascribed to the higher reducibility, the lower oxidation state of Ni NPs and the enhanced hydrogen spillover of Ni to the support. Moreover, the Ni/NCB catalyst is relatively cheap and easy scale-up production, thus achieving a low-cost transformation of biomass to bio-oils.

Introduction

Biomass represents renewable alternatives to fossil-fuel resources for the green production of liquid fuels and valuable chemicals.¹ For example, lignin can be broken down to phenolic compounds (called bio-oil) by various approaches.² Bio-oil usually contains up to 60 wt% oxygen, an upgrading process is necessary to reduce the oxygen content, and improve the heating value and the stability.³ Up to date, several approaches, hydrodeoxygenation (HDO),⁴⁻⁸ cracking⁹ and aqueous-phase reforming¹⁰ on zeolite have been developed for the bio-oil upgrading. Among all practicable routes mentioned above, catalytic HDO is a very promising process because this route can achieve high conversion efficiency with low emission.

Undoubtedly, the precious metal-based catalysts still remain leading for HDO such as palladium,^{11, 12} platinum,^{13, 14} rhodium,¹⁵ ruthenium^{4, 16} and aurum-based^{17, 18} systems, even though their widespread applications are limited by low earth-abundance and high cost. Among the non-noble catalysts, a number of studies have been reported on the activity of unmodified and modified (using alkaline and precious metals) Co-Mo and Ni-Mo catalysts^{15, 19-22} for HDO, dehydrogenation and hydrogenolysis of model molecules

representative of bio-oils. However, the non-noble-metal catalysts usually exhibit relatively low activity, require higher temperatures (150-300 °C) and hydrogen pressures (2-7 MPa), consume more energy in the process. Additionally, the conventional Al₂O₃ is not a good support because it tends to deactivate very fast (irreversibly undergoes partial crystallization to form boehmite), in which water is formed in the HDO reaction,²³ and the presence of weak Lewis acid sites on the alumina support benefits the coke formation.²⁴ Therefore, alternative heterogeneous Ni catalysts with improved performance for HDO of biomass under mild conditions are desired.

Carbon can offer many advantages as the support because of its good resistance to acid and base media, low cost and high thermal stability.²⁵ Most importantly, carbon has less affinity to produce coke as compared to the acidic supports for HDO reactions.²¹ However, the weak interaction of NPs with carbon can lead to aggregation or leaching, which inevitably reduces the catalytic activity. Moreover, it has hardly any surface species, making it a non-preferred choice for reactions needing acid-base functionality, such as the hydrogenolysis of carbon-oxygen bonds.²⁶ To overcome this limitation, the functionalization of carbons is necessary in most cases.

Recently, nitrogen-doped carbon materials with rich pore structure and excellent electrical conductivity have been recognized as superior candidates as catalyst supports and catalytic materials.²⁷ It is envisioned that N-doped carbon supported metal NPs as the catalyst for heterogeneous catalysis would exhibit enhanced performance because of the following reasons. (1) The N-dopants in the carbon skeleton can be usually regarded as favorable anchoring sites or defects for enhancing the particle nucleation and reducing the particle size.²⁸ (2) The N doping results in an

Hubei Collaborative Innovation Center for Advanced Organic Chemical Materials, & Ministry-of-Education Key Laboratory for the Synthesis and Application of Organic Functional Molecules, School of Chemistry and Chemical Engineering, Hubei University, Wuhan 430062, P.R. China.
E-mail: d.zhou@hubu.edu.cn (D. Zhou); xiaqh518@aliyun.com (Q. H. Xia);
Fax/Tel: +86 27 88662747

† Electronic Supplementary Information (ESI) available: Additional experimental results. See DOI: 10.1039/x0xx00000x

ARTICLE

Journal Name

improvement in the hydrophilicity and basicity of supports,²⁹ beneficial to the use of the prepared catalysts in aqueous phase and the sufficient interaction of substrate with support. (3) The introduction of N can modify the electronic structure of carbon matrix, and tune the activity of the sp^2 carbon and metal NPs in the H_2 activation by lowering down the dissociation energy,^{30,31} thus promoting the catalytic hydrogenation. However, recent studies on the promoting effect of N-doped carbon support have mainly focused on noble metals and on the comparison of oxygen and nitrogen functional groups.^{11,32} It is of great interest to know whether the promoting effect can be applied to non-noble metals, especially to those oxidized easily in air.

As a model molecule, vanillin (4-hydroxy-3-methoxybenzaldehyde, a common component of pyrolysis oil) can be effectively hydrogenated into 2-methoxy-4-methylphenol (MMP), which is a potential future biofuel.^{4, 11, 12, 33, 34} However, the HDO of vanillin normally requires noble metal catalyst, high hydrogen pressure and high temperature, and always forms by-product (4-hydroxymethyl-2-methoxyphenol, HMP) as a result of incomplete hydrogenation due to the low catalytic activity of catalysts. Herein, we have synthesized porous N-doped CB for constructing supported Ni catalyst for the HDO of vanillin. The type and amount of functional groups on the surface of CB are tuned, and the properties and catalytic performance of the supported Ni NPs for catalytic hydrogenation are also discussed.

Results and discussion

Characterizations of nanostructured N-doped carbon materials

Firstly, the morphology and structure of NCB is studied. The SEM images (Fig. S1) show no obvious differences in the morphology between pristine CB and N-doped CB, suggesting the homogeneity of N species on surface of CB. Nitrogen sorption analysis of CB and NCB (Fig. 1) show H_4 hysteresis loop on the isotherm and sharp rise at relative pressure higher than 0.80, characteristic of textural mesopores.³⁵ As expect, the average pore sizes of NCB-900, NCB-600, CB and AC are calculated to be 16.4, 16.8, 15.0 and 4.3 nm, respectively (Table 1). It can be seen that, after N-doping of CB, the S_{BET} increases from 87.7 to 103.1 m^2/g for NCB-600, and further increases to 137.9 m^2/g for NCB-900, probably owing to the emission of many non-carbon or carbon elements and enhancement of the burn off of CB@polypyrrole when the carbonization temperature increases.³⁶

The FTIR spectra of NCB (Fig. S2) show characteristic peak at 1384 cm^{-1} related to C–N heterocycles,³⁷ which fluctuates weakly with increasing the temperature. The C1s peak of NCB (Fig. S3) shows a tail peak at high binding energy of around 285–290 eV, is assigned to the electron-deficient carbons bind to nitrogen/oxygen (C=N/C–N and C–O).³⁸ The percentages of nitrogen (Table S1) in

Table 1 Pore structure of the supports.

Supports	S_{BET} (m^2/g)	V_{total} (cm^3/g)	Average pore diameter (nm)
NCB-900	137.9	0.372	16.8
NCB-600	103.1	0.386	16.4
CB	87.7	0.455	15.0
AC	718.5	0.44	4.3

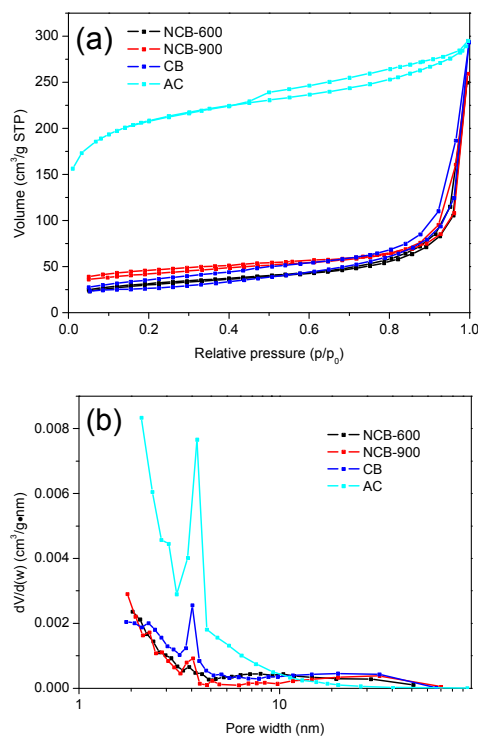


Fig. 1 (a) Nitrogen sorption isotherms and (b) pore size distributions of the supports.

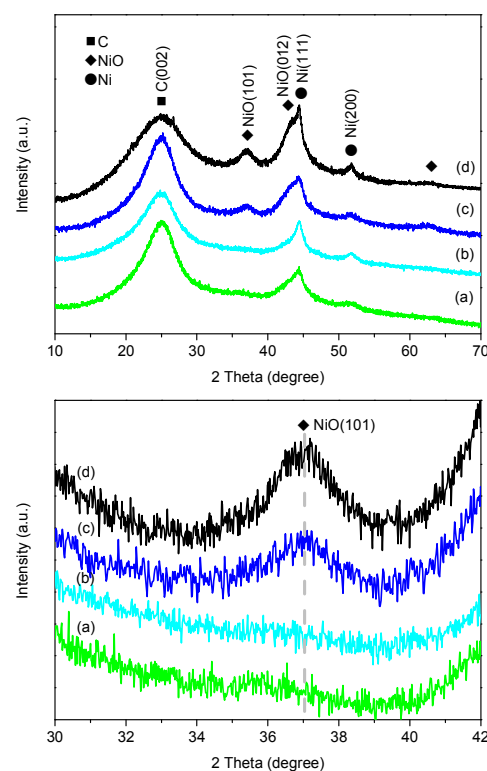


Fig. 2 The XRD patterns of (a) Ni/NCB-900, (b) Ni/NCB-600, (c) Ni/CB and (d) Ni/AC.

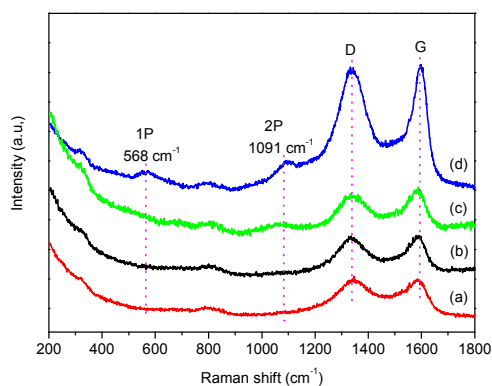
Table 2 Structural properties of N-doped carbon materials.

Catalysts	Particle size (nm)		Relative atomic percentage (%)		N1/N2	Relative atomic percentage (%)	
	XRD	TEM	N1 (398.5 eV)	N2 (400.5 eV)		Ni ⁰	Ni ²⁺
Ni/NCB-600	8.1	8.7	50.1	49.9	1.0	15.6	84.4
Ni/NCB-900	7.7	8.1	63.6	36.4	1.75	13.3	86.7
Ni/CB	8.3	9.1	-	-	-	3.8	96.2
Ni/AC	8.4	9.7	-	-	-	3.0	97.0

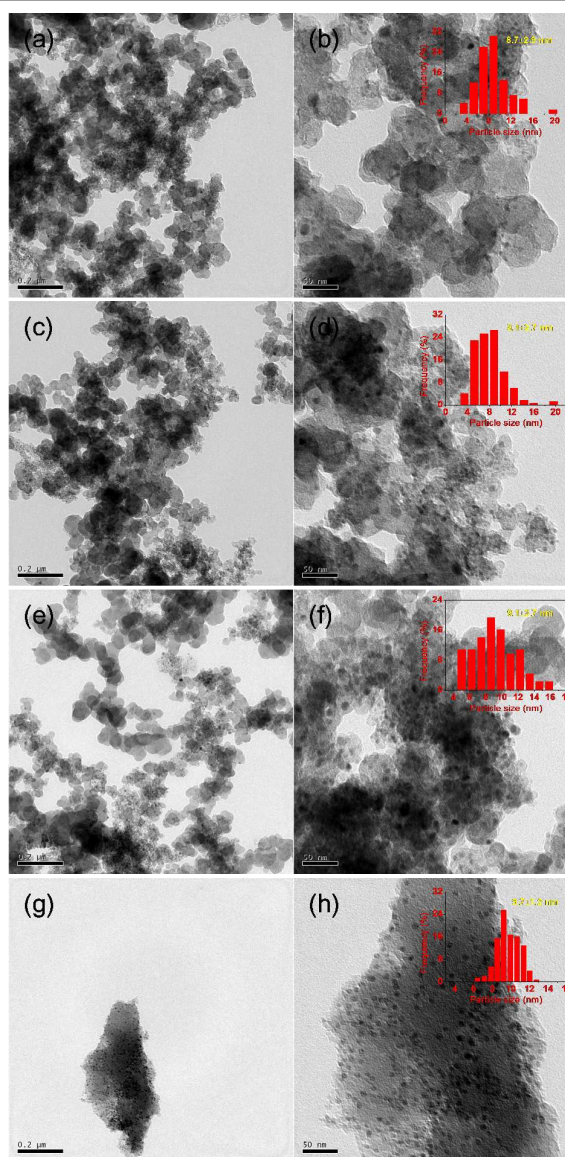
Ni/NCB-600 and Ni/NCB-900 are calculated from the XPS survey spectra to be around 4.38 and 2.98 am%, respectively, implying the partial removal of N species from carbon skeleton.

In order to characterize the Ni NPs on carbon surface, XRD, TEM and XPS *et. al* have been carried out. Typical XRD patterns of Ni-based catalysts are shown in Fig. 2. The broad characteristic peak at around 24.3° is ascribed to the (002) plane reflection of carbon. The intensive diffraction peaks at 44.5° and 51.8° are associated with the (111) and (200) planes of the face-centered-cubic (fcc) structure Ni (PDF# 04-0850), respectively.²⁶ The crystallite sizes of Ni calculated by Scherrer equation are also listed in Table 2. The crystallite size of Ni supported on NCB is smaller than that of Ni supported on AC, suggesting that the N-doping of CB can promote the dispersion of Ni. Moreover, Ni/CB and Ni/AC catalysts show two strong peaks at 2θ values of 37.3 and 43.3° , corresponding to the (101) and (012) planes of NiO,²⁶ while these NiO peaks weaken for Ni/NCB-900 and even disappear for Ni/NCB-600. This result indicates that higher reduction of NiO to metallic Ni could occur on surface of nitrogen-doped supports.

The Raman spectra of Ni-based catalysts are presented in Fig. 3, in which the G band at $\sim 1590\text{ cm}^{-1}$ indicates the in-plane vibration of sp^2 carbon atoms,³⁹ while the D band at $\sim 1350\text{ cm}^{-1}$ is a defect-induced Raman feature representing the imperfect crystalline structure of carbon.⁴⁰ Compared with the Ni/CB, the I_D/I_G value shows an increase from 0.91 to 1.02 and 1.07 for Ni/NCB-900 and Ni/NCB-600, respectively, indicating the formation of much more structural defects on N-doped CB. The Ni/CB and Ni/AC catalysts show multiple Raman peaks of NiO between 500 and 1200 cm^{-1} . The peaks observed at 568 and 1091 cm^{-1} are ascribed to one-phonon (1P) and two-phonon (2P) light

**Fig. 3** The Raman spectra of (a) Ni/NCB-900, (b) Ni/NCB-600, (c) Ni/CB and (d) Ni/AC.

scattering,⁴¹ well agreed with the XRD results. As demonstrated by XRD and Raman, clear decrease of the NiO intensity and increase of metallic Ni dispersion occur due to the increase of nitrogen content from 0 to 4.38 at% on surface of CB (Table S1).

**Fig. 4** TEM images of (a, b) Ni/NCB-600, (c, d) Ni/NCB-900, (e, f) Ni/CB and (g, h) Ni/AC. The insets in images (b, d, f and g) are corresponding histograms of Ni particle size distribution.

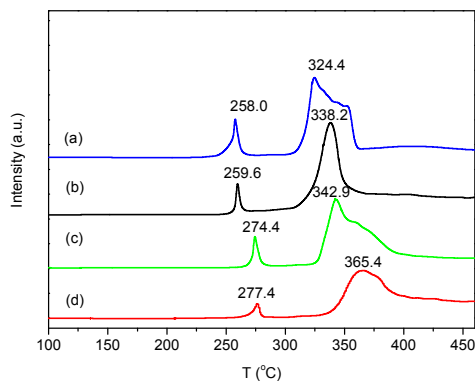


Fig. 5 The H₂-TPR spectra of (a) Ni/NCB-600, (b) Ni/NCB-900, (c) Ni/CB and (d) Ni/AC.

Fig. 4 shows the TEM images and particle size distributions of Ni catalysts. It can be seen that the particle size of Ni NPs is in range of 3–20 nm without substantial differences on these three CB supports. However, Ni particles are not so well-dispersed and agglomerate more or less on N-free CB support, whereas the particle size on NCB seems to be more homogeneous, and large particles are seldom detected, which can be attributed to the strong anchoring effect of surface N groups in accordance with previous reports.^{42,43} Comparatively, the Ni NPs on AC seem to be more uniform with a narrow size distribution than those on CB, which can be ascribed to rich micropore structure for size confinement.⁴⁴ Statistical analysis of the particle size is carried out by measuring the size of ca. 150 Ni NPs, which yields the histograms shown in Fig. 4. It can be found that the average Ni sizes with standard deviation in Ni/NCB-600, Ni/NCB-900, Ni/CB and Ni/AC are 8.7±2.9, 8.1±2.7 nm, 9.1±2.7 and 9.7±1.2, respectively, well agreed with the XRD results.

TPR results can reveal the reduction behavior of Ni²⁺ species (Fig. 5). Two peaks are observed at temperature lower than 400 °C in TPR profiles of the four dried samples. The first peaks in all samples are very similar in terms of peak shape and peak intensity, ascribing to the decomposition of nickel precursor. However, the position of the first peak for Ni/NCB-600 and Ni/NCB-900 is shifted to a lower temperature of ca. 258 °C, as compared to ca. 277.4 °C for Ni/CB and Ni/AC, indicating the promoting effect of the surface nitrogen

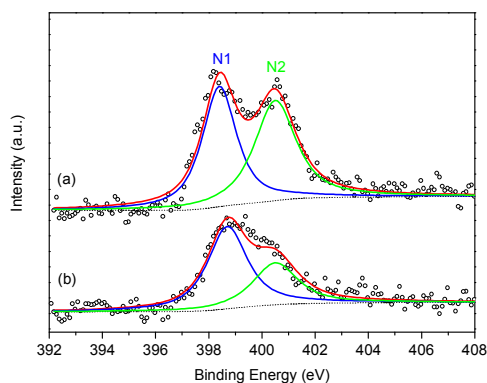


Fig. 6 The N1s spectra of (a) Ni/NCB-600 and (b) Ni/NCB-900. on the decomposition of nickel precursor.⁴² The second peak centered at ca. 320–370 °C is found in four TPR profiles due to the reduction of nickel oxides (formed through precursor decomposition) to metallic Ni. In addition, the second peak for Ni/AC centered at ca. 365.4 °C is higher than that of 342.9 °C for Ni/CB. This peak is further shifted to lower temperature of ca. 338.2 and 324.4 °C for Ni/NCB-900 and Ni/NCB-600, respectively. Comparatively, the relatively narrow peak for Ni/NCB-900 indicates well-dispersed Ni species on surface of NCB. The electron-donating effect of surface N species, as observed in several previous studies, is assumed to be responsible for the promoting effect.^{45,46} Besides, the metal cations are believed to be preferably located on N-containing sites on the carbon surface, which possess modified local electronic structure likely favoring the reduction of supported Ni.⁴² In case of Ni/NCB-600 with a higher surface N content, the local electronic structure can be more significantly modified, leading to a more pronounced promoting effect.

The N envelope (Fig. 6) demonstrates that the nitrogen atoms are mainly in form of pyridinic N (N1, 398.2 eV) and pyrrolic N/N-Ni (N2, 400.4 eV).⁴⁷ It can be seen that, for Ni/NCB-600, N1 and N2 account for 50.1 and 49.9 % in total N atoms, respectively. In terms of Ni/NCB-900, the intensity of the N1 peak becomes much stronger and its proportion is obviously higher (63.6 %) than that of Ni/NCB-600, indicating the formed N1 is much more stable than N2 at high temperatures.³⁶ These results demonstrate that N atoms within the pentagonal ring of polypyrrole are progressively converted to type of N1 in the carbonization process, as previously found in other materials.

The surface chemistry of the Ni-based samples after reduction at 400 °C is examined using XPS (Fig. 7). The main Ni 2p_{3/2} peaks for all samples are found to be at 854.5 eV, revealing that surface Ni is mainly in the oxidized state.⁴⁸ In the case of Ni/NCB-900 and Ni/NCB-600, a minor contribution is recorded at a lower binding energy of 852.7 eV, which can be assigned to Ni in metallic state. For example, the metallic Ni percentages (Table 2) in Ni/NCB-900 and Ni/NCB-600 are 13.3 and 15.6 %, respectively, much higher than that of Ni/CB (3.8 %) and Ni/AC (3.0 %). The presence of metallic Ni confirms the stabilization effect of the NCB support as revealed by the XRD analysis.

Previous results in the literature suggested that pyridinic N sites

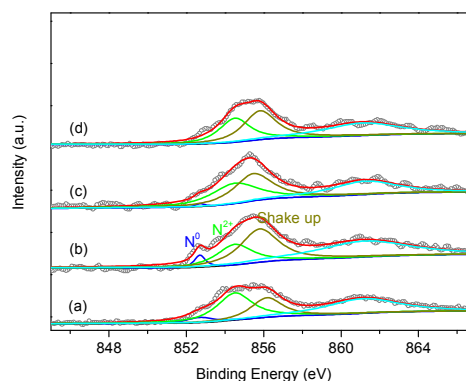


Fig. 7 Ni2p spectra of (a) Ni/NCB-900, (b) Ni/NCB-600, (c) Ni/CB and (d) Ni/AC.

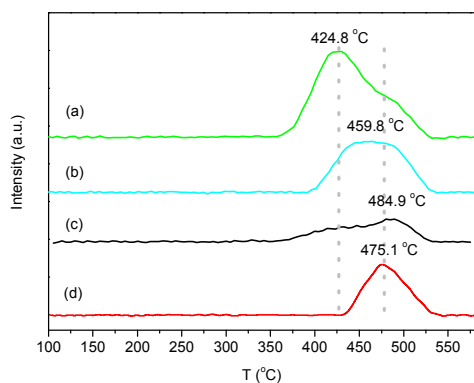


Fig. 8 The H₂-TPD spectra of (a) Ni/NCB-900, (b) Ni/NCB-600, (c) Ni/CB and (d) Ni/AC.

could facilitate both the coordination of metal ions and the anchoring of metal NPs to their electron-withdrawn property.⁴⁹ XPS spectra show that pyridinic nitrogen atoms exist dominantly in NCB, which are often associated with defect sites on edges of graphite layers or on vacancy sites.⁵⁰ It was reported that the interaction of Co with pyridinic nitrogen atom would lead to the increased electron density of the Co atoms through Co-N-C(III) structure as compared to the Co-N(II) precursor.⁵¹ As expected, compared with NCB-900 (Fig. S5), the N1 peak in Ni/NCB-900 becomes weak. For instance, the N1 proportions in NCB-900 and Ni/NCB-900 are 81.5 and 63.6 %, respectively. This result indicates that the N1 atom donates preferentially electron to Ni NPs, which leads to the shift of N1 binding energy to high-energy side and the increase of N2 proportion in Ni/NCB-900.⁵² Therefore, it can be concluded that the XPS-detectable metallic Ni arises mainly from the Ni atoms bonded to pyridinic N atoms in the carbon skeleton.

H₂-TPD tests of Ni catalysts are carried out (Fig. 8). The profiles of all show a broad desorption peak centered between 300–550 °C. As for Ni/AC and Ni/CB catalyst, the peaks appear at 475.1 and 484.9 °C, respectively. Although the peak intensity of Ni/CB is fairly weak compared to those in Ni/AC, a peak shoulder shows up at ~425 °C for Ni/CB, suggesting the spillover hydrogen on CB due to its high

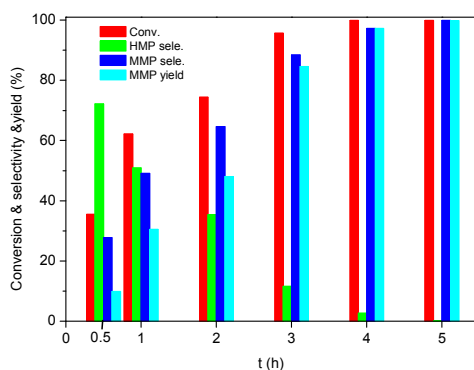


Fig. 9 Time-activity profile for the selective hydrogenation of vanillin over Ni/NCB-900. Reaction conditions: Vanillin (228 mg), Ni/NCB-900 (20 mg), H₂O (10 mL), 0.5 MPa H₂, 150 °C.

graphitized carbon skeleton.⁵³ Moreover, the signal peaks of hydrogen desorption in Ni/NCB-600 and Ni/NCB-900 strengthen obviously. In case of Ni/NCB-900, the TPD profile exhibits a more strengthened shoulder at 424.8 °C, suggesting more obvious spillover hydrogen in N-doped CB.⁵⁴ It should be considered whether the signal peak is caused by a size effect of Ni NPs, namely that smaller Ni usually has stronger signal peak. In this work, the size effect is unlikely to be the only origin of peak area. For example, although Ni/NCB-600 has much stronger signal peak than Ni/CB, its particle size of Ni is close to that of Ni/CB. Moreover, Ni/AC has a stronger signal peak than Ni/CB, while its particle size is larger than that of Ni/CB. And, there is no clear relationship between peak intensity and Ni size. Therefore, the peak intensity can also be attributed to spillover hydrogen of Ni to support.⁵⁰ Here, it can be found that N-doping pushes up the capacity of CB for hydrogen spillover, and higher treatment of NCB owns stronger hydrogen spillover ability.³⁰

Catalytic property of Ni catalysts

The HDO of vanillin in water is carried out as a model reaction. Fig. 9 displays the evolution of the vanillin and products with the time over Ni/NCB-900. In the initial stage of the reaction, vanillin is transformed to HMP with a relatively moderate rate, and about 35.5 % conversion of vanillin is obtained within 0.5 h. When the reaction time prolongs, the reaction is accelerated and almost 95.7 % conversion of vanillin is obtained at 3 h. As the reaction continues, the concentration of HMP decreases gradually, while the concentration of MMP increases correspondingly. Further reacting for 2 h, HMP is converted completely with a 99.8 % MMP yield. It is worth mentioning that no other product is observed during the whole process. These results demonstrate that vanillin is mainly reacted with H₂ by hydrogenation of C=O bond to form HMP and further deoxidized to form MMP in water.

The impact of solvent on hydrogenation of vanillin is investigated under the similar condition (Fig. 10). Among these solvents examined, the reaction in water shows the best activity for vanillin hydrogenation, giving 74.4 % conversion of vanillin and 48.1 % yield towards MMP after 2 h. We deduce that, doping with N atoms increases the hydrophilic property of Ni/NCB-900, which might

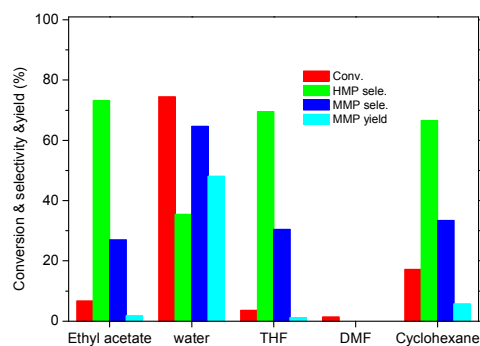
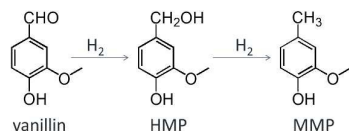


Fig. 10 Hydrogenation of vanillin in different solvents over Ni/NCB-900. Reaction conditions: Vanillin (228 mg), Ni/NCB-900 (20 mg), solvent (10 mL), 0.5 MPa H₂, 150 °C, 2 h.

ARTICLE

Journal Name

Table 3 The aqueous phase HDO of vanillin over different Ni-based catalysts.^a

Entry	Catalysts	Conversion / %	Selectivity / %		MMP yield / %
			HMP	MMP	
1	No catalyst	1.2	-	-	-
2	Ni/NCB-600	52.9	39.4	60.6	32.1
3	Ni/NCB-900	74.4	35.4	64.6	48.1
4	Ni/CB	37.8	49.4	50.6	19.1
5	Ni/AC	35.9	75.2	24.8	8.9
6	Ni/SiO ₂	0.3	-	-	-
7	Ni/MgO	19.0	1.4	98.6	18.7
8	Ni/ZrO ₂	3.7	79.5	20.5	0.8
9	2nd reuse of entry 3	78.1	34.9	65.1	50.8
10	3rd reuse of entry 3	72.3	32.5	67.5	48.8
11	4th reuse of entry 3	71.1	35.5	64.5	45.9
12	5th reuse of entry 3	68.7	37.2	62.8	43.1

^a Reaction conditions: vanillin (228 mg), catalyst (20 mg), H₂O (10 mL), 0.5 MPa H₂, 150 °C, 2 h.

enhance the catalyst dispersion in water and improve the exposure of the catalyst to the substrates. The reaction in ethyl acetate, THF and cyclohexane obtains relative low vanillin conversion (3.6–17.2 %) with the desired MMP selectivity of 26.9–33.4 %. Additionally, the reaction in DMF exhibits nearly no transformation of vanillin.

The HDO of vanillin in water over different Ni catalysts is tested and these results are summarized in Table 3. In blank test, when no catalyst is used, nearly no vanillin is transformed (entry 1). Under 150 °C and low hydrogen pressure of 0.5 MPa for 2 h, the conversion of vanillin reaches 52.9, 74.4, 37.8 and 35.9 % over Ni/NCB-600, Ni/NCB-900, Ni/CB and Ni/AC, respectively (entries 2–5), indicating the significant improvement towards activity *via* N-doping of carbon. Although similar vanillin conversion can be achieved over Ni/CB and Ni/AC, the desired MMP selectivity over Ni/CB (50.6 %) is much higher than that of Ni/AC (24.8 %), which might be ascribed to the micropore-free structure of CB that is beneficial for smooth transformation of HMP. The calculated MMP yield over Ni/NCB-900 is 5.4 times higher than that of Ni/AC. Other frequently used heterogeneous Ni-based catalysts inclusive of Ni/SiO₂, Ni/MgO and Ni/ZrO₂ (entries 6–8) achieve poor hydrogenation activity or MMP selectivity under the same condition. These results imply that the nature of support has a noticeable impact on the catalytic activity of Ni for vanillin hydrogenation and Ni/NCB-900 is a good hydrogenation catalyst in water.

The NCB-900 supported Ni catalysts with different Ni content are prepared and investigated for HDO of vanillin (as shown in Table S2). It can be found that vanillin conversion is quickly increased from 48.1 to 90.8 % after 2 h when the Ni loading is increased from 4.95 to 19.45 wt %. However, the TOF value based on total Ni atoms exhibits a reverse variation trend with increasing the Ni loading from 4.95 to 19.45 wt %, in which the maximal value of 21.4 h⁻¹ is achieved over 4.95 % Ni/NCB-900. Moreover, as the Ni loading

increases, the specific MMP yield of per Ni atom is enhanced slightly from 10.1 to 11.6 h⁻¹ as increasing the Ni loading from 4.95 to 7.41 wt %. Further increasing the Ni loading to 19.45 wt %, however, leads to significant decrease of this value to 7.5 h⁻¹. Therefore, lower Ni loading could accelerate the transformation of vanillin, while moderate Ni loading could give the highest efficiency for MMP generation over single Ni atom.

Using Ni/NCB-900 as catalyst, we can still achieve 51.2 % conversion of vanillin and 42.8 % selectivity of MMP even decreasing the temperature to 130 °C. When the hydrogenation of vanillin is carried out under higher temperature (190 °C), the MMP yield is 99.8 % (Fig. S6). High yield of MMP (>99.5 %) can also be realized by decreasing the substrate dosage (from 228 to 76 mg, Fig. S7) or increasing the hydrogen pressure (from 0.5 to 2.5 MPa, Fig. S8). The Ni/NCB-900 catalyst can be easily separated by extraction and recycled 5 times with a small fluctuation of activity or MMP selectivity (Table 3, entries 9–12). ICP-AES analysis of the reaction mixture and the used catalyst did not detect the leaching of any metal during recycling, also proven by the characterization of the reused catalyst (Fig. S9 and S10).

Based on these experimental results above, the improved catalytic activity of Ni/NCB catalysts could be attributed to several factors. Firstly, the rich surface nitrogen (Table S1) results in good hydrophilic property that benefits the dispersion of catalyst in water and the wettability of the substrate on support, hence accelerating the diffusion and transformation of substrates.⁷ Secondly, the incorporated nitrogen facilitates the highly dispersion and stabilization of Ni NPs on the surface of carbon supports (Fig. S2 and 4). The electron-rich nitrogen donates electron to Ni NPs preferably than carbons,²⁶ leading to high electron density on Ni surface (Fig. 7) and easy reduction of Ni species (Fig. 5). It is confirmed that the catalytic activity and selectivity of the catalyst can be ascribed to Ni(0) species. The stronger interaction between Ni NPs and nitrogen species on surface of carbon affords catalytically active sites for vanillin hydrogenation. Thirdly, the hydrogen spillover effect of catalyst has been greatly enhanced through the metal-support interface due to the N-doping of carbon skeleton, as is confirmed by H₂-TPD analysis. It is well known that hydrogen spillover exerts a great influence on the catalytic activity in hydrogenation reactions.³⁰ In one word, the greatly improved catalytic activity of Ni/NCB-900 can also be ascribed to its increased interfacial sites, which enhance the hydrogen spillover effect (Fig. S11).

Conclusions

Porous nitrogen-doped carbon black is synthesized by facile carbonization using CB as template and pyrrole as nitrogen source. Using NCB as support for Ni NPs, the as-obtained catalyst exhibits high performance for hydrogenation of vanillin to MMP under mild conditions, which is significantly superior to other frequently-used nickel-based catalysts. The high catalytic activity can be ascribed to the specific characteristics of the nanostructure of Ni/NCB and the intimate interaction of Ni NPs and N species, endowing Ni with the higher reducibility, hydrogen spillover and the lower oxidation state. Moreover, the Ni/NCB catalyst is not only cheap but also easily separable, and therefore, this approach facilitates achieving the cost-effective reduction of vanillin to bio-oils.

Experimental

Materials

The chemicals used included pyrrole (98 %, Sinopharm), Ni(NO₃)₂•6H₂O (98 %, Sinopharm), ammonium persulfate (APS, 98 %, Sinopharm), H₂O₂ (30 %, Sinopharm), vanillin (99.5 %, Aladdin). Vulcan XC-72 carbon black (CB) was purchased from Cabot Corporation. Active carbon (AC) was purchased from Hunan Xiangda Chemical Reagent Co. All other chemicals were of analytical purity if not otherwise noted.

Preparation of NCB

Ten grams of carbon black (CB) was first immersed in 250 mL H₂O₂ (28 wt%) solution. The slurry was stirred and treated at 50 °C for 5 h. Then, the solid was recovered by filtration and washed thoroughly with distilled water. The pretreated CB was dried in a vacuum oven at 80 °C for 10 h, which is denoted as H₂O₂-CB. In a typical synthesis of NCB, 500 mL of the 90.3 mmol/L pyrrole aqueous solution was added into 1.0 g H₂O₂-CB followed by 30 min of sonication. The mixture was then stirred for 60 min before it was transferred into a beaker. Subsequently, 200 mL of aqueous APS solution (45.3 mmol/L) was slowly added into the beaker under continuous stirring at 30 °C. After further stirring for 4 h, the product CB@polypyrrole was separated by filtration, washed with ethanol and water, and dried at 60 °C overnight under vacuum. Finally, the CB@polypyrrole was annealed in a quartz tube under N₂ atmosphere with a 5 °C/min heating rate to carbonization temperature (600 and 900 °C) for 2 h to obtain the nitrogen-doped CB (NCB-600 and NCB-900).

Preparation of NCB supported Ni catalysts

NCB-supported Ni NPs were prepared by impregnation using Ni(en)₃(NO₃)₂ as precursor (en, ethylenediamine).⁵⁶ Briefly, 50 mL of Ni(en)₃(NO₃)₂ aqueous solution (0.034 mol/L) and 1 g of NCB were mixed at 30 °C for 2 h. Dark powders were obtained after removing water in a rotary evaporator, and the powders were dried in a vacuum oven at 80 °C for 10 h. The sample was subsequently calcined in nitrogen at 300 °C for 90 min, followed by reduction in H₂ atmosphere at 400 °C for 120 min, yielding the Ni/NCB catalyst. Other two different samples with the same nominal loading of 10 wt% (weight percent) were prepared by using CB and AC as supports and designated as Ni/CB and Ni/AC.

Catalyst characterization

Powder X-ray diffraction (XRD) was performed on a Bruker D8A25 diffractometer with CuKα radiation (λ = 1.54184 Å) operating at 30 kV and 25 mA in the range of 10–80° 2θ. N₂ adsorption was carried out at -196 °C using an auto-adsorption analyzer (Micromeritics, TriStar II). Before adsorption measurements, the samples were degassed at 250 °C overnight under vacuum. The total pore volume was determined from the aggregation of N₂ vapor adsorbed at a relative pressure of 0.99. The specific surface area was calculated by using the Brunauer–Emmett–Teller (BET) method, and the pore size distributions were measured by using Barrett–Joyner–Halenda (BJH) analysis from the desorption branch of the isotherms. Raman

spectra were collected at room temperature from 100 to 4000 cm⁻¹ with 514.5-nm argon ion laser (Rhenishaw Instruments, England). The spectra were recorded at a resolution of 2 cm⁻¹. X-ray photoelectron spectra (XPS) were recorded on a Perkin-Elmer PHI ESCA system. Scanning electron images (SEM) and surface compositions were collected on JEOL (JSM6700F) with an accelerating voltage of 15 kV. Transmission electron microscope (TEM) images were obtained using an accelerating voltage of 200 kV on a JEOL-135 2010F Transmission Electron Microscope.

TPR experiments were performed in a flow setup using 20 vol% H₂ in N₂ at a flow rate of 50 mL/min. The TPR of the calcined Ni/NCB samples was performed from room temperature to 600 °C at a heating rate of 5 °C/min. A thermal conductivity detector (TCD) was used to monitor the H₂ consumption. Before starting the TPR procedure, the sample was pretreated at 200 °C for 30 min in a N₂ flow of 100 mL/min and then cooled down to room temperature.

The H₂ activation activity of the reduced catalysts was detected *via* temperature-programmed desorption of H₂ (H₂-TPD). The sample was first reduced at 400 °C in a H₂ flow of 30 mL/min for 1 h, purged in purified N₂, and further treated at 450 °C for 0.5 h in N₂. Then the reactor was cooled to 30 °C in N₂, exposed to 20% H₂/N₂ for 30 min, and purged with by N₂ for 2 h at 30 °C in order to eliminate the physically adsorbed H₂. H₂-TPD was conducted by ramping to 650 °C at 5 °C/min and H₂ in effluent was detected and recorded by a thermal conductivity detector (TCD).

Selective HDO of vanillin

The catalytic test was carried out in a 50 mL stainless autoclave with a Teflon liner. In a typical procedure, 20 mg catalyst was dispersed in 10 mL DI water, and then added with 228 mg vanillin. The autoclave was sealed, purged and pressurized with hydrogen to 0.5 MPa, and then heated to 150 °C under magnetic stirring at a rate of 1000 rpm. After reaction, the autoclave was quickly cooled down within cold water. The organic compounds was extracted by ethyl acetate, the catalyst was recovered from aqueous phase by centrifugation and then washed several times with ethanol. The contents of products and substrate were analyzed by gas-chromatogram (Shimadzu 2010) with a 30 m capillary column (Rtx[®]-1) using a flame ionization detector (FID). Interpolated calibration was employed for product quantification using standard solutions of vanillin, HMP and MMP. All the products were confirmed by GC-MS (Agilent 6890).

Acknowledgements

This work was supported by National Natural Science Foundation of China (21603066, 21673069, 21503074, 21571055), Natural Science Fund for Creative Research Groups of Hubei Province (2014CFA015), Natural Science Fund of Hubei Province (2015CFB232), the 2014 Sci-tech Support Project of the Science and Technology Department of Hubei Province (2014BAA098), Natural Science Fund of the Education Department of Hubei Province (Q2015009), and Hubei Provincial Outstanding Youth Foundation (2016CFA040).

Notes and references

ARTICLE

Journal Name

1. R. Sharma and N. Bakhshi, *Energy & Fuels* 1993, **7**, 306-314.
2. A. Singh, D. Pant, N. Korres, A. Nizami, S. Prasad and J. Murphy, *Bioresour. Technol.*, 2010, **101**, 5003-5012.
3. F. H. Mahfud, S. Bussemaker, B. J. Kooi, G. H. Ten Brink and H. J. Heeres, *J. Mol. Catal. A* 2007, **277**, 127-136.
4. S. Crossley, J. Faria, M. Shen and D. Resasco, *Science* 2010, **327**, 68-72.
5. H. Lee, H. Kim, M. J. Yu, C. H. Ko, J.-K. Jeon, J. Jae, S. H. Park, S.-C. Jung and Y.-K. Park, *Sci. Rep.*, 2016, **6**, 28765-28773.
6. H. Lee, Y.-M. Kim, I.-G. Lee, J.-K. Jeon, S.-C. Jung, J. D. Chung, W. G. Choi and Y.-K. Park, *Korean J. Chem. Eng.*, 2016, **33**, 3299-3315.
7. H. W. Lee, B. R. Jun, H. Kim, D. H. Kim, J.-K. Jeon, S. H. Park, C. H. Ko, T.-W. Kim and Y.-K. Park, *Energy* 2015, **81**, 33-40.
8. E. H. Lee, R.-s. Park, H. Kim, S. H. Park, S.-C. Jung, J.-K. Jeon, S. C. Kim and Y.-K. Park, *J. Ind. Eng. Chem.*, 2016, **37**, 18-21.
9. B. Puértolas, T. C. Keller, S. Mitchell and J. Pérez-Ramírez, *Appl. Catal. B* 2016, **184**, 77-86.
10. T. Vispute and G. Huber, *Green Chem.*, 2009, **11**, 1433-1445.
11. X. Xu, Y. Li, Y. Gong, P. Zhang, H. Li and Y. Wang, *J. Am. Chem. Soc.*, 2012, **134**, 16987-16990.
12. Z. Zhu, H. Tan, J. Wang, S. Yu and K. Zhou, *Green Chem.*, 2014, **16**, 2636-2643.
13. X. Chen, L. Zhang, B. Zhang, X. Guo and X. Mu, *Sci. Rep.*, 2016, **6**, 28558-28571.
14. L. J. Durndell, C. M. A. Parlett, N. S. Hondow, M. A. Isaacs, K. Wilson and A. F. Lee, *Sci. Rep.*, 2015, **5**, 9425-9434.
15. Y.-C. Lin, C.-L. Li, H.-P. Wan, H.-T. Lee and C.-F. Liu, *Energy & Fuels* 2011, **25**, 890-896.
16. G. Yao, G. Wu, W. Dai, N. Guan and L. Li, *Fuel* 2015, **150**, 175-183.
17. Y. Zhu, H. Qian, B. A. Drake and R. Jin, *Angew. Chem. Int. Ed.*, 2010, **49**, 1295-1298.
18. S. Zhu, Y. Xue, J. Guo, Y. Cen, J. Wang and W. Fan, *ACS Catal.*, 2016, **6**, 2035-2042.
19. J. Bredenberg, M. Huuska, J. Raty and M. Korpio, *J. Catal.*, 1982, **77**, 242-247.
20. W. Wang, L. Li, S. Tan, K. Wu, G. Zhu, Y. Liu, Y. Xu and Y. Yang, *Fuel* 2016, **179**, 1-9.
21. S. Mukundan, M. Konarova, L. Atanda, Q. Ma and J. Beltramini, *Catal. Sci. Technol.*, 2015, **5**, 4422-4432.
22. M. Ferrari, B. Delmon and P. Grange, *Carbon* 2002, **40**, 497-511.
23. E. Furimsky and F. E. Massoth, *Catal. Today* 1999, **52**, 381-495.
24. E. Laurent and B. Delmon, *Stud. Surf. Sci. Catal.*, 1994, **88**, 459-466.
25. J. Xia, G. He, L. Zhang, X. Sun and X. Wang, *Appl. Catal. B* 2016, **180**, 408-415.
26. X. Kong, Y. Zhu, H. Zheng, X. Li, Y. Zhu and Y.-W. Li, *ACS Catal.*, 2015, **5**, 5914-5920.
27. X. Wang, G. Sun, P. Routh, D.-H. Kim, W. Huang and P. Chen, *Chem. Soc. Rev.*, 2014, **43**, 7067-7098.
28. R. Nie, M. Miao, W. Du, J. Shi, Y. Liu and Z. Hou, *Appl. Catal. B* 2016, **180**, 607-613.
29. E. Haque, J. W. Jun, S. N. Talapaneni, A. Vinu and S. H. Jung, *J. Mater. Chem.*, 2010, **20**, 10801-10807.
30. T. Fu, M. Wang, W. Cai, Y. Cui, F. Gao, L. Peng, W. Chen and W. Ding, *ACS Catal.*, 2014, **4**, 2536-2543.
31. Z. Wei, J. Wang, S. Mao, D. Su, H. Jin, Y. Wang, F. Xu, H. Li and Y. Wang, *ACS Catal.*, 2015, **5**, 4783-4789.
32. X. Cui, A.-E. Surkus, K. Junge, C. Topf, J. Radnik, C. Kreyenschulte and M. Beller, *Nat. Commun.*, 2016, **7**, 11326-11334.
33. M. T. Jimaré, F. Cazaña, A. Ramirez, C. Royo, E. Romeo, J. Faria, D. E. Resasco and A. Monzón, *Catal. Today* 2013, **210**, 89-97.
34. X. Yang, Y. Liang, Y. Cheng, W. Song, X. Wang, Z. Wang and J. Qiu, *Catal. Commun.*, 2014, **47**, 28-31.
35. A. Vinu, *Adv. Funct. Mater.*, 2008, **18**, 816-827.
36. L.-F. Chen, *ACS Nano* 2012, **6**, 7092-7102.
37. Q. Hu, M. C. Paau, Y. Zhang, X. Gong, L. Zhang, D. Lu, Y. Liu, Q. Liu, J. Yao and M. M. F. Choi, *RSC Adv.*, 2014, **4**, 18065-18073.
38. G. P. Mane, S. N. Talapaneni, C. Anand, S. Varghese, H. Iwai, Q. Ji, K. Ariga, T. Mori and A. Vinu, *Adv. Funct. Mater.*, 2012, **22**, 3596-3604.
39. V. Chandra, J. Park, Y. Chun, J. W. Lee, I.-C. Hwang and K. S. Kim, *ACS Nano* 2010, **4**, 3979-3986.
40. H. Wang, X. Xiang and F. Li, *J. Mater. Chem.*, 2010, **20**, 3944-3952.
41. P. K. Nayak, C. Hsu, S. Wang, J. C. Sung and J. Huang, *Thin Solid Films* 2013, **529**, 312-316.
42. P. Chen, F. Yang, A. Kostka and W. Xia, *ACS Catal.*, 2014, **4**, 1478-1486.
43. M. Shalom, V. Molinari, D. Esposito, G. Clavel, D. Ressnig, C. Giordano and M. Antonietti, *Adv. Mater.*, 2014, **26**, 1272-1276.
44. R. Nie, H. Jiang, X. Lu, D. Zhou and Q. Xia, *Catal. Sci. Technol.*, 2016, **6**, 1913-1920.
45. X.-H. Li and M. Antonietti, *Chem. Soc. Rev.*, 2013, **42**, 6593-6604.
46. G. Zhang, S. Zang, L. Lin, Z.-A. Lan, G. Li and X. Wang, *ACS Appl. Mater. & Interfaces* 2016, **8**, 2287-2296.
47. H. Jiang, X. Yu, X. Peng, H. Q. Zhang, R. Nie, X. Lu, D. Zhou and Q. Xia, *RSC Adv.*, 2016, **6**, 69045-69051.
48. T. Zeng, H. Zhang, Z. He, J. Chen and S. Song, *Sci. Rep.*, 2016, **6**, 33348-33357.
49. X. Ning, H. Yu, F. Peng and H. Wang, *J. Catal.*, 2015, **325**, 136-144.
50. Y. Zhou, K. Neyerlin, T. S. Olson, S. Pylypenko, J. Bult, H. N. Dinh, T. Gennett, Z. Shao and R. O'Hayre, *Energ. Environ. Sci.*, 2010, **3**, 1437-1446.
51. F. Chen, A.-E. Surkus, L. He, M.-M. Pohl, J. Radnik, C. Topf, K. Junge and M. Beller, *J. Am. Chem. Soc.*, 2015, **137**, 11718-11724.
52. D. A. Bulushev, M. Zacharska, E. V. Shlyakhova, A. L. Chuvilin, Y. Guo, S. Beloshapkin, A. V. Okotrub and L. G. Bulusheva, *ACS Catal.*, 2016, **6**, 681-691.
53. P. A. Gordon and R. B. Saeger, *Ind. Eng. Chem. Res.*, 1999, **38**, 4647-4655.

Journal Name

ARTICLE

54. Z. Gao, M. Dong, G. Wang, P. Sheng, Z. Wu, H. Yang, B. Zhang, G. Wang, J. Wang and Y. Qin, *Angew. Chem. Int. Ed.*, 2015, **54**, 9006-9010.
55. T. Mokrane, A. Boudjahem and M. M. Bettahar, *RSC Adv.*, 2016, **6**, 59858-59864.
56. J. Wang, Z. Yuan, R. Nie, Z. Hou and X. Zheng, *Ind. Eng. Chem. Res.*, 2010, **49**, 4664-4669.

Graphic abstract



Porous nitrogen-doped carbon black (NCB) derived from carbon black (CB) and pyrrole was used as support for Ni NPs. The catalyst exhibited significantly higher activity than most of Ni-based catalyst for selective HDO of vanillin in aqueous phase at mild conditions, which was ascribed to the higher reducibility, the lower oxidation state of Ni NPs and the enhanced spillover hydrogen of Ni to NCB due to the intimate interaction of Ni and N species.